UNDERSTANDING THE LASER SINTERTING OF POLYMERS AT MICROSCALE LEVEL BY USING X-RAY COMPUTED TOMOGRAPHY

Michele PAVAN[1, 2], Tom CRAEGHS[1], Jean-Pierre KRUTH[2], Wim DEWULF[2]

[1]Materialise NV; Technologielaan 15, 3001 – Leuven, Belgium; E-mail:
michele.pavan@materialise.be, tom.craeghs@materialise.be

[2] Department of Mechanical Engineering, KU Leuven; Celestijnenlaan 300, 3001 - Leuven, Belgium;
E-mail: jean-pierre.kruth@kuleuven.be , wim.dewulf@kuleuven.be

Abstract

Literature reports on many cases where X-ray Computed Tomography (CT) has been used to measure the porosity of laser sintered (LS) polymeric parts, in order to characterize the process parameters' influence on their density. However, this approach implies to perform a CT scan for each parameter set being assessed, making the evaluation very costly and time consuming. Moreover, this approach does not provide useful information about the coalescence steps of the process and the local variation of the powder packing density which happen at the microscale level, namely at dimensions comparable to the layer thickness used during the process. This work presents a new CT-based approach which allows to assess at the microscale the variation of the sintering conditions for several scanning strategies at the same time. The study focuses on PA12 powder, but the proposed approach is general and can potentially be applied to every laser sinterable polymeric powder.

Introduction

Additive Manufacturing (AM) processes are increasingly moving from the production of prototypes to end-users functional parts. Among the AM polymer processes Laser Sintering (LS) is the most promising to meet the quality requirements needed and to become a genuine manufacturing technique. However, some aspects of the LS process still need to be improved, in order to reduce the spread in part quality, to reduce the overall porosity levels, and to improve the robustness of the process [1].

Due to the strict requirements imposed by the laser sintering process the number of processable materials is still limited compared with the wide variety of materials available for industrial processes like Injection Molding (IM) [1-2]. Materials used in laser sintering are normally semi-crystalline, with polyamide-12 (PA12) dominating the laser sintering powders market with a share around 90%. Nevertheless during the last years an increasing number of materials have been introduced, and there is a crescent research focus on the development of new powders and determination of suitable process conditions to process them [1]. Powder bed pre-heating temperature, sintering window of the polymer and process energy density are particularly important to achieve a successful sintering, but unfortunately their values differ a lot polymer to polymer [3]. Table 1 resumes the typical values of pre-heating temperature and energy density used to process some commercially available sinterable polymeric powders.

Table 1 Typical values of pre-heating temperature and energy density used to process some commercially available sinterable polymeric powders.

Material	Pre-heating temperature (°C)	Surface Energy Density (J/mm^2)	Volumetric Energy Density (J/mm^3)	Reference
TPU	95	0.0304	-	[2]
PA12	~170	-	0.25	[4]
PEEK	~300	0.026-0.030	-	[5]
PP	105	0.0458	-	[6]

Although the different laser sinterable polymers present a big variability in term of process conditions, their consolidation during the process is always conducible to a partial or full melting of the powder particles, with a densification driven by the reduction of the system's surface energy through the viscous flow of the polymer [3]. Experimental studies confirm the great importance of the zero shear viscosity in the sintering behavior under hot stage [7, 2], which is a property that differs a lot among the laser sinterable polymers and even between virgin and re-used powders of the same polymer [8].

Due to this properties variability, finding good processing conditions for new laser sintering materials is difficult and requires a considerable research effort. Even more difficult is making a link between the process parameters used, the internal porosity and the mechanical properties. Even for PA12, which is a well-known laser sintering material with plenty of literature available, there are still some problems to reach low porosity levels and isotropic mechanical properties [9]. It is clear that a better understanding of the process physics happening at the microscale level is needed to speed up the selection of the process parameters, to reach an efficient bonding between the layers and to reduce the number of defects in the polymer microstructure, all of which are a direct result of the process parameters and the scanning pattern used. For this purposes CT proves to be a very suitable tool, because of its capabilities to inspect and measure internal defects of an object in a non-destructive way [10]. Literature provides a number of cases where CT-based porosity measurements have been used to characterize quantitatively and qualitatively the porosity present in LS polymeric parts. Rouholamin et al. [11] performed a CT-based porosity measurement on cut PA12 disks produced by LS using different laser powers. Ghita et al. [12] used CT to qualitatively compare the porosity levels of PEK samples produced using different mixing ratios between virgin and used powder. Ruesenberg et al. [13] used X-ray CT to make a qualitative comparison of the porosity levels between different regions of the samples. The authors observed that the skin of the sample appeared to be always denser than the internal regions, independently if the contours vectors were being scanned or not. Previous research by the authors [14-17] has moreover shown how the data obtained by X-ray CT can be used to assess the influence of the different parameter sets and the scanning pattern on the porosity content and on its distribution in the printed parts. The method previously developed consists of simple tools based on image processing of CT-slices, which allow to visualize the porosity distribution along the slicing direction, and permit the creation of cumulative porosity maps useful to determine the most affected areas in the parts.

The aim of this work is to be able to assess the laser sintering process for different scanning strategy at the microscale level, separating the influence of the laser parameter set from the scanning pattern used, as well as assessing the effect of local variation of the powder packing density. The work performed is divided in three different sections. In the first part of the paper we present additional tools based on image processing of CT slices that allow to estimate the sintered layers' thickness and to determine possible variation of process conditions during the printing. Case studies which make use of these tools are presented, showing how

different process parameters lead to a different stability of the sintering conditions at the layer level. In the second part of the study, a new approach is presented. This method makes use of a new test object to assess the process at the microscale level allowing to directly assess the bonding between the layers for different parameter sets at the same time, to measure the powder packing density as well as its intra-and-inter-layer variation in different regions of the part. In the last part of the paper, a second test object which allows to assess the effect of up to 16 scanning strategies at the same time is proposed to investigate the effect of the scanning pattern on the porosity content and to spot the most affected areas. All tests have been carried out on PA2200 powder from EOS GmbH with a 50-50 mixing ratio between new and re-used powder. However the methodology presented can be extended to other polymeric powders with the advantage to potentially reduce the machine time and material costs needed for the selection of the scanning strategy (parameter set + scanning pattern) to process a new material, making benefit of the limited size of the samples needed for the test and the fast multi-scanning-strategy assessment.

Methods

1. **Influence of the parameters sets on the variation of the sintering conditions at the layer thickness level**

    The results presented in the following section are divided into three parts: an initial part shows how applying the tools based on image processing of CT-slices allows to assess the influence of the LS process parameters on the microstructure, especially focussing on determining variation of the sintering conditions at the layer thickness level during the printing process. The test is carried out using a cubic sample with 10mm side produced using a P395 machine from EOS GmbH and the parameters sets reported in Table 2. Figure1 shows the x-y cross scanning pattern used to manufacture the samples. The specimen's geometry ensures an equal length of the x-and-y hatching's vectors, allowing to assess only the influence of the parameter sets of the scanning strategies tested.

Table 2 Parameters' sets used to produce the PA12 cubic samples of 10 mm side using a laser sintering P395 machine from EOS GmbH, and relative porosity values measured using x-ray CT.

ID sample	Contour Power (W)	Contour Scan Speed (mm/s)	Contour Energy Density (J/mm)	Hatching Laser Power (W)	Hatching Scan Speed (mm/s)	Hatching Scan Spacing (mm)	Energy Density (J/mm2)	Porosity CT (%)
N1	34	3000	0.0113	44.0	4190	0.3	0.0350	3.48
N2	34	3000	0.0113	30.8	4190	0.3	0.0245	4.45
N6	34	3000	0.0113	44	5986	0.3	0.0245	4.74
N7	34	3000	0.0113	44	4929	0.3	0.0298	3.79
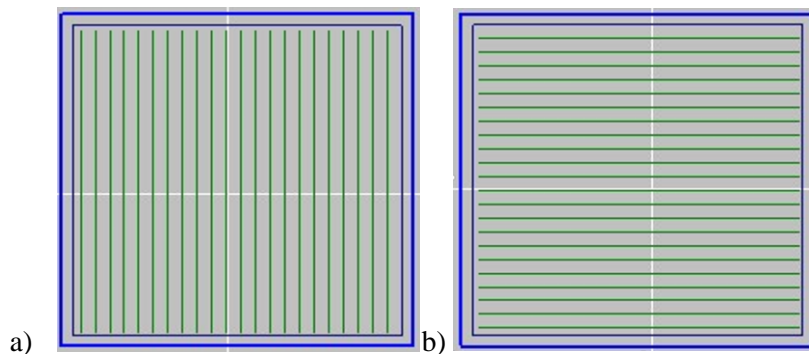
Figure 1 a) x and b) y cross scanning pattern used to produce the samples reported in Table 2.

2. Assessment of the local powder packing density and layer bonding efficiency

The second part of the work focusses on the study of the process at microscale level assessing both the layer bonding for several parameter sets and the powder packing density variation both intra-layer and inter-layer in different region of the part. This study is carried out using the test object shown in Figure 2a which consists of a hollow cube of 10 mm side with a wall thickness of 1 mm. Inside it contains 6 replicas of a stair-like object with the thickness of the steps respectively equal to 1, 2, 3 and 4 times the layer thickness. The central part of the object remains unsintered on purpose, enabling to assess the packing of the powder. The specimens are produced in a state-of-the-art laser sintering machine, which has been equipped with the new Materialise Control Platform (MCP) [18], using the same scanning pattern for all the replicas. The first test object is manufactured using the parameters sets reported in Table 3.

Table 3 Parameters sets used to produce the internal replicas of the test object reported in Figure 1 a).

ID Parameter Set	Contour Power (W)	Contour Scan Speed (mm/s)	Contour Energy Density (J/mm)	Hatching Laser Power (W)	Hatching Scan Speed (mm/s)	Hatching Scan Spacing (mm)	Hatching Energy Density (J/mm²)
1	34	3000	0.0113	45	4000	0.3	0.0375
2	34	3000	0.0113	28.125	2500	0.3	0.0375
3	34	3000	0.0113	11.25	1000	0.3	0.0375
4	34	3000	0.0113	40	4000	0.3	0.0333
5	34	3000	0.0113	25	2500	0.3	0.0333
6	34	3000	0.0113	10	1000	0.3	0.0333

a)   b)
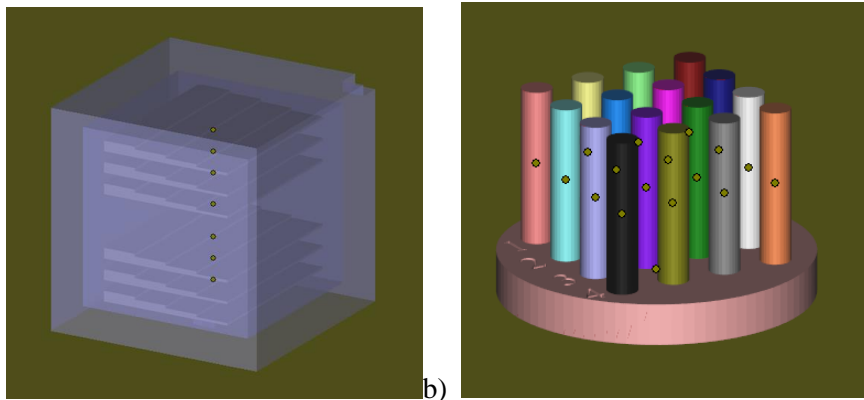
Figure 2 a) First test object used to assess the influence of different parameters sets on the layer bonding and the powder packing density. b) Second test object used to assess the influence of the scanning pattern on the porosity content and its distribution.

3. Influence of the scanning pattern on the porosity characteristics

The third part of the study aims to investigate the influence of the scanning pattern on the porosity content and its local distribution for several scanning strategies. The investigation is performed using a second test object shown in Figure 2b which contains 16 cylinders 15mm tall with a diameter of 3mm, which according to [16] presents porosity characteristics similar to the bulk. In this test 4 scanning patterns have been tested in combination with 4 different parameters test (selected among the one used to test carried out in the second part), yielding to 16 different scanning strategies tested at once. The specimen is produced in a state-of-the-art laser sintering machine, which has been equipped with the new Materialise Control Platform (MCP). MCP is interfaced with a dedicated build processor which provides a wider choice of scanning patterns compared to commercial laser sintering machines. Figure 3 shows the scanning patterns used to produce the second test object with a reference to the scanning order and parameters sets used which are respectively reported in Table 3 and 4.
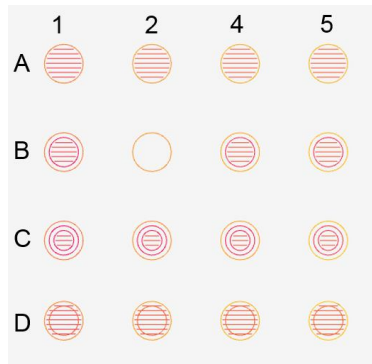
Figure 3 Array of scanning patterns used to produce the second test object with references to the scanning order and the parameters sets used which are reported respectively in Table 2 and Table 3. *There was an error in the settings of the scanning pattern relative to the position B2.

Table 4 Addition information about the scanning pattern and scanning order used to produce the test object reported in Figure 1b).

ID Scanning Pattern	Number of Contours	Scanning Order	Notes
A	1	Hatchings; External contour	No overlap between vectors
B	2	Internal contour; Hatchings; External contour	No overlap between vectors
C	3	Internal contours, Hatchings; External contour	No overlap between vectors
D	2	Hatchings; Internal contour; External contour	Overlap between internal contour and hatchings

All the samples presented in this paper are made starting from a PA2200 PA12 powder from EOS GmbH with a mixing ratio 50/50 between virgin and re-used powder and a layer thickness of 120 microns. All test samples have been printed at the center of the build platform in order to minimize the influence of the uneven temperature distribution and to warrant equal sintering times.

X-ray Computed Tomography

All CT scans have been performed using a 225 kV CT machine from Nikon Metrology using a Molybdenum target, a voltage of 110 kV, a current of 127 μA and 3000 projections. The magnification used for the different samples ranges from x22 to x10 depending on their size leading to a voxel size between 9.11 and 20 μm, which according to [14] ensures a sufficiently accurate porosity measurement. The reconstruction of the projections into the voxel volume (float 32 bit format) is performed using CT Pro 3D software from Nikon Metrology. The datasets are analyzed using VGstudio max v. 2.2 from Volume Graphics GmbH, where the closed porosity is calculated using the defect detection module; for the defect detection analysis the 'only threshold' algorithm has been used, measuring pores which contained a minim of 8 voxels, in order to avoid erroneous estimation influenced by the dataset noise. In order to determine the porosity distribution and the areas which are most affected, image processing on the CT-slices is performed. An important step in this analysis is the volume alignment with the original STL file used to print the object, which allows to export the slices aligned with the printing direction (see Figure 4).

Results and Discussion

1. **Influence of the parameters sets on the variation of the sintering conditions at the layer thickness level**

   Figure 5 shows the porosity distribution along the printing direction (Figure 5c) and along a direction parallel to the powder bed platform (Figure 5b) of the sample N2 (see Table 2). The small voxel size (9.11 µm) achieved in the CT scan allows a high points statistic, hence a good description of the porosity distribution within the part. It clearly shows how the porosity distribution along the printing direction presents a regular variation compared to in-plane directions. Figure 5d shows a detail, which give an idea about the magnitude of the intra-and-inter-layer variations along the printing direction. Figure 5b and c show how the porosity close to the borders is lower, confirming that the skin of the parts are denser as found by Ruesenberg et al. [13]. Figure 4b also shows that the porosity reaches a peak close to the border, followed by a sudden drop before reaching a more stable distribution inside the part.
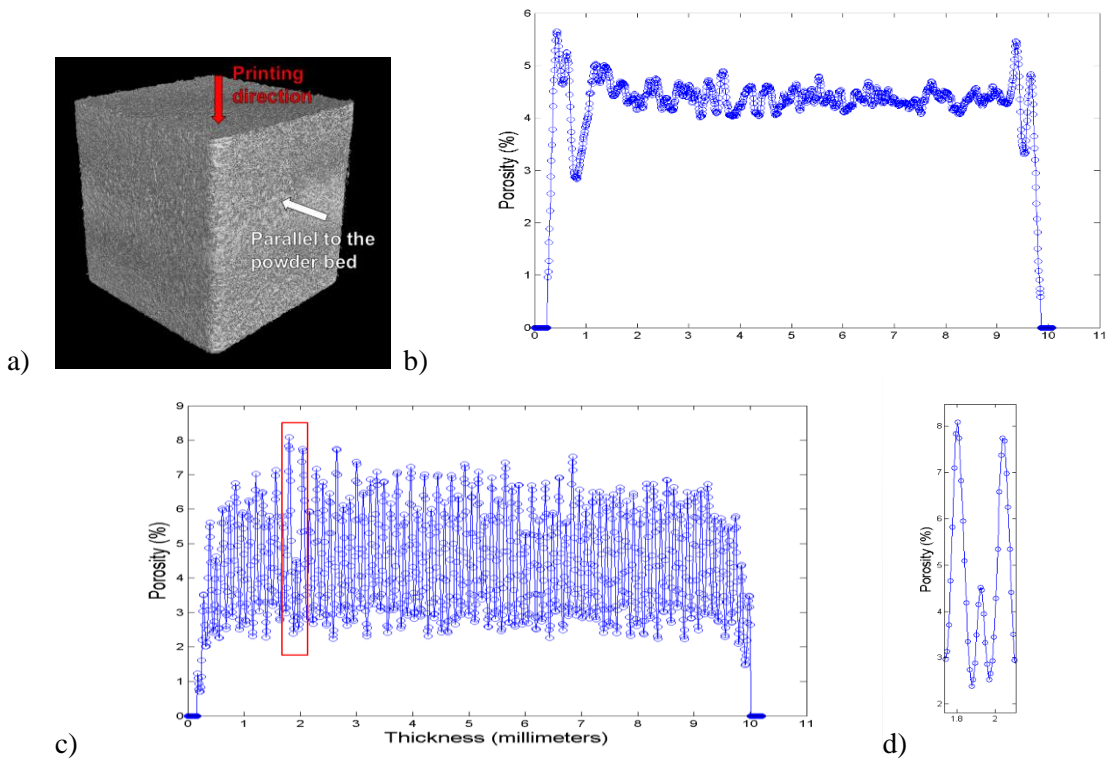
Figure 5 a) View of the sample with reference to the different directions; b) Porosity distribution along the direction parallel to the powder bed platform and c) along the printing direction related to the sample N2 in Table 2; d) Detail of the porosity distribution along the printing direction (red rectangle in c).

Applying the Fourier Transform to the regular pattern of the porosity distribution along the printing direction shown in Figure 5c allows to analyze the periodicity of the porosity variation. The number of slices per nominal layer thickness, calculated by dividing the nominal layer thickness by the voxel size of the CT scan, is used as sampling frequency.

a)   b)
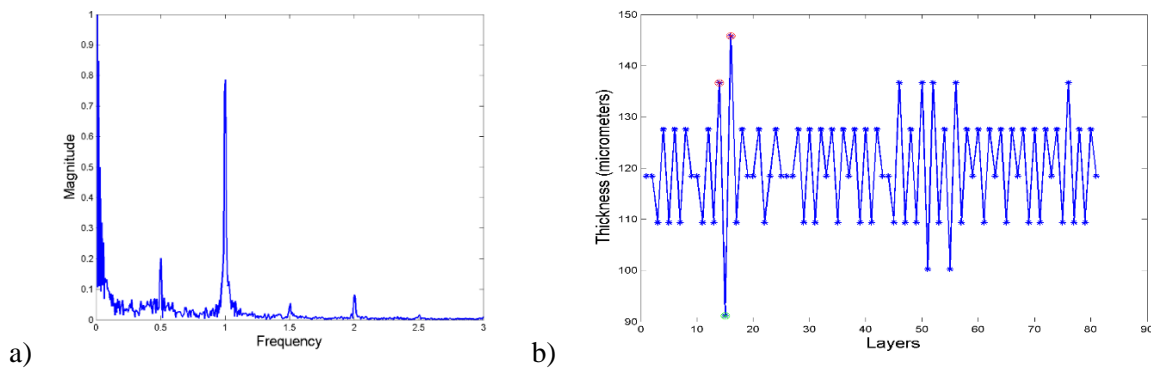
Figure 6 a) Fourier transform of the porosity distribution along the printing direction of sample N2 (Table 2) shown in Figure 5c; b) Estimated layer thickness of the sample whose porosity distribution is shown in Figure 5c, with the red and green asterisks indicating the layers corresponding to the detail of the porosity distribution in Figure 5d).

The peak at 1 shown in Figure 6a represents a periodicity of the porosity distribution corresponding to every layer, confirming that for the sintering conditions used, there is always a more porous region in the layer. The peak at 0.5 implies that there is an additional variation occurring every second layer. This peak appears to be present in most of the samples analyzed (see also Figure 7) with a variable magnitude depending on the process parameters used. This unexpected effect means that the process runs under different conditions every second layer. This analysis is however useful to assess both the magnitude of the porosity variation and the question whether the sintering conditions maintain constant during the entire printing process. The main effect of the printing process of PA12 is a regular porosity variation along the printing direction, with the pores mainly concentrated between the layers. Looking at the detail of the porosity distribution in Figure 5d, it can be observed that the distances peak-to-valley and valley-to-peak are similar. What one would expect is to have the porosity mainly concentrated at the bottom of the layers, due to the fact the laser is shining from the top inducing a gradient of temperature from top to bottom as predicted in the simulation results in [19]. With this gradient of temperature, it could be expected to have a more efficient sintering at the top of the layers and a less efficient sintering at the bottom of the layers, which would probably result in a gradient of porosity from top to bottom of each layer. A possible explanation for this profile of the porosity distribution might be found in the average pore size, which according to [14] is around 150 microns, namely of the same order of magnitude of the layer thickness. Another possible cause might be an uneven packing density of the powder intra-layer and inter-layer, which might influence locally the resulting density of the sintered material (the local variation of the packing density will be further investigated in the second part of the study).The porosity distribution periodicity with a wave length of one layer thickness shown in Figure 6a suggests that it is possible to estimate the thickness of each sintered layer by counting the number of slices between 2 minima (or 2 maxima) and multiplying it by the voxel size achieved in the CT scan (the CT-slices are spaced by a dimension equivalent to the voxel size). Figure 6b shows the layers' thickness estimation for the porosity distribution in Figure 5c. It is clear that the layer thickness is oscillating around 120 microns, which is the nominal layer thickness value. Also this effect suggests that the printing process might run under different conditions every second layer. Figure 7 shows porosity distributions of samples manufactured using different Energy Densities (EDs). One can observe how an increase in ED reduces the spread between peaks and valleys of the porosity distribution, leading for sample N1 (Figure 7c) to a less evident periodicity. Overall an increase in ED leads to a progressively lower average porosity value, improving the connection between the layers and reducing the anisotropy of the sample. Observing the relative Fourier transforms in Figure 7d one can see that the peak at 0.5 progressively decreases in magnitude by increasing the ED. This is especially evident when

comparing sample N6 and N7, which have the same magnitude of the peak at 1, but a very different magnitude of the sample at 0.5. This behavior suggests the process might be more subject to instabilities for low ED values.

a)   b)

c)   d)
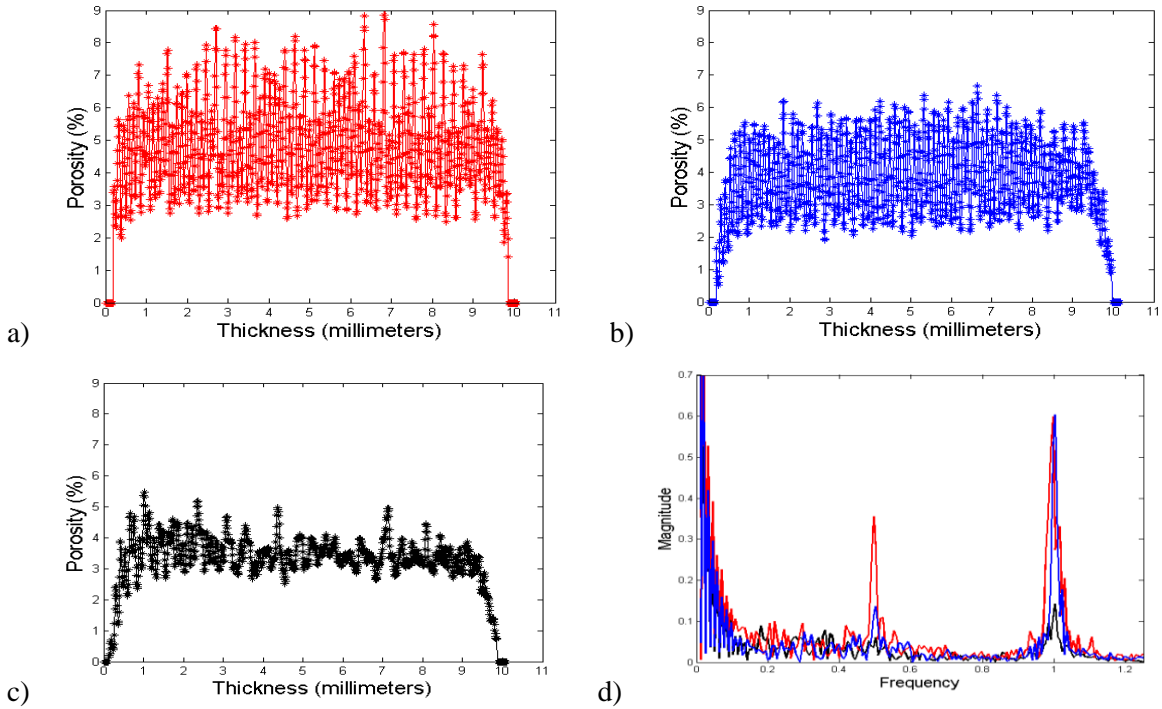
Figure 7 a) Porosity distribution along the printing direction for samples N6 (ED=0.0245J/mm²) a), N7 (ED=0.0298J/mm²) b) and N1 (ED=0.0350J/mm²) c) (Table 2), with the relative Fourier transform d).

2. Assessment of the local powder packing density and layer bonding efficiency

Figure 8 shows the workflow which leads from the STL model of the first test object to the map which represents the percentage porosity content along the slicing direction.
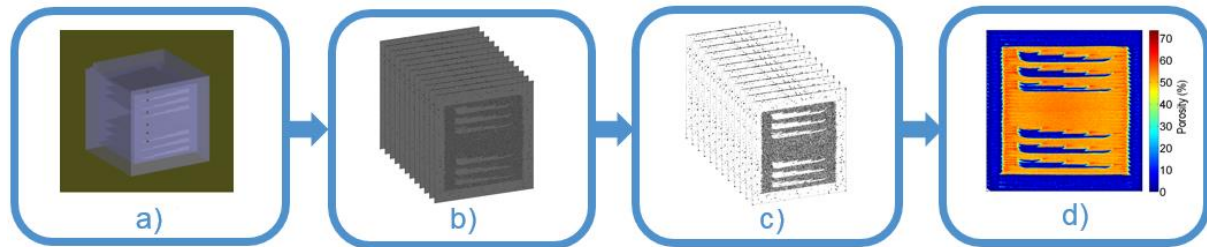
Figure 8 Workflow from the STL model of the first test object for the evaluation of the percentage of porosity content in the sintered replicas and in the packed powder. a) STL model of the first test object; b) CT-slices exported along a direction parallel to the main axes of the internal replicas; c) CT-slices binarized used to calculate the porosity content in each slice; d) Map which resumes all the information of each slice about the percentage of the voids content along the slicing direction.

Figure 9 shows both the STL (a) and the map (b) relative to the percentage of the voids content along the slicing direction. This map allows to assess both the bonding between the layers for 6 different parameters sets as well as the powder packing density in different areas. The reference to the parameter sets (see Table 3) used to manufacture each replica are indicated in Figure 9a. Each group of 3 replicas (top and bottom) are produced using the same energy density (2 different values in total), but using different laser power for each replica and adapting accordingly the scanning speed. Figure 9b shows that, for both energy density values, the bonding between the layers decreases when the power and speed are lowered. This is probably due to a not sufficient penetration depth for low laser powers used (parameters sets 3 and 6, see Table 3). All the 6 replicas present a marked warpage close to the border of each layer, which

seems to badly influence the local powder packing density. The same effect is noticeable close to the wall of the hollow cube, with a more marked effect for powder located between the wall and a replica.
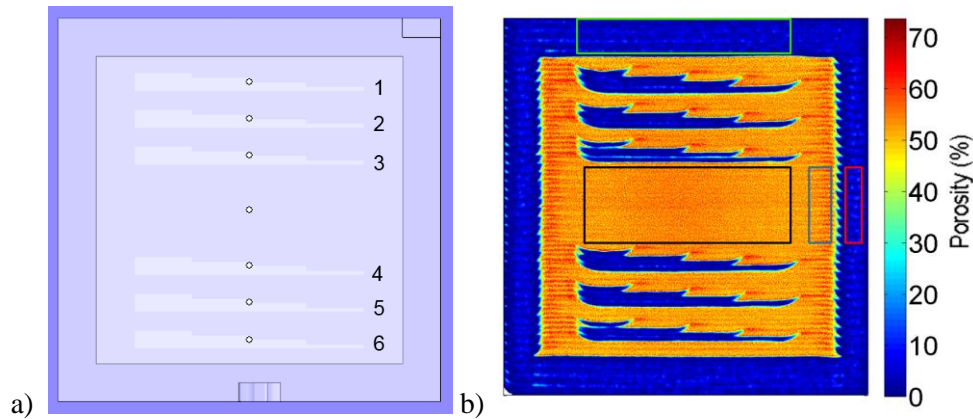
Figure 9 a) STL model of the first test object constituted by a hallow cube of 10 mm side with a wall thickness of 1 mm which contains 6 replicas of a stair-like object with the thickness of the steps respectively equal to 1, 2, 3 and 4 times the layer thickness. b) Map showing the percentage of porosity along the slicing direction. In the map are shown 4 areas where porosity and packing density will be further analyzed.

In order to further investigate this variation, 2 different areas located at the same height are selected in the map shown in Figure 9b: a central (black rectangle) and a side (blue rectangle) areas used to assess the average powder packing density, its variation intra-and-inter-layer. The calculated average value of the packing density in the central and side areas are respectively 46.51 % and 46.15%, which are in agreement with typical values reported in literature [20]. In order to assess the local variation of the powder packing density, the average profile along the height is calculated in both areas and shown in Figure 10a.
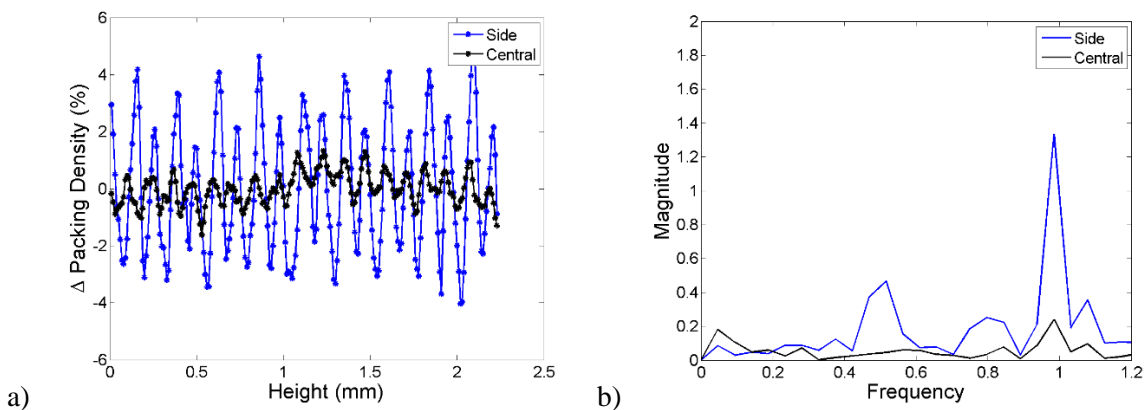
Figure 10 a) Variation of the packing density relative to the areas highlighted in the Figure 9b obtained subtracting to the distributions the relative average powder packing density values; b) Fourier transform of (a) obtained using the layer thickness as sampling frequency.

The powder packing density profile of the central area shows an oscillating behavior with a maximum of the packing density in the middle of the layer; in fact the distances valley-to-peak and peak-to-valley look comparable. Although the average powder packing density of the two areas (central and side) are very close, their profiles differ significantly; in fact the profile of the side area presents a much higher oscillation compared to the central one. For both profiles the intra-layer variation is probably due to the difficulty to achieve an efficient packing of the powder at the bottom of the layer, which for the area close to the already sintered material (side area) become more intense. The inter-layer variation seems not significant for the central area, while for the side area becomes marked. This latter effect is probably due to the recoating direction, which leads to more efficient powder packing density in one direction compared to

the other. The described periodicities of the oscillations are confirmed by the Fourier transform shown in Figure 10b, which is calculated using a sampling frequency equal to the layer thickness.

In Figure 9b are also indicated 2 regions of sintered material: one at the top of the hollow cube (green rectangle) and another one on the wall (red rectangle). The porosity profile of the top region (see Figure 11a) presents periodicities at 1 and 0.5 (see Figure 11b) indicating a variation of the sintering conditions every second layer, with the single layers still distinguishable. Assuming the original powder packing density in this region to be similar to the one of the central area shown in Figure 10a, the variation of the porosity profile cannot be attributed to this effect. The probable cause of this effect has to be researched in the parameter set used, which could have leaded to a variation of the sintering conditions similar to what already described in the first part of the study (see Figure 7). On the other end the porosity profile of the sintered region in the wall shows only a periodicity every second layer, with the porosity of 2 layers resulting to be merged. Figure 11c and d show the cross scanning pattern used to manufacture the walls of the hollow cube, indicating a big difference in the length of the hatching's vectors in the two directions of scanning, which could be probably the cause of the effect. A similar behavior of the porosity distribution was already found in previous research [17] when using an ED equal to 50J/mm2.

a)   b)

c)   d)
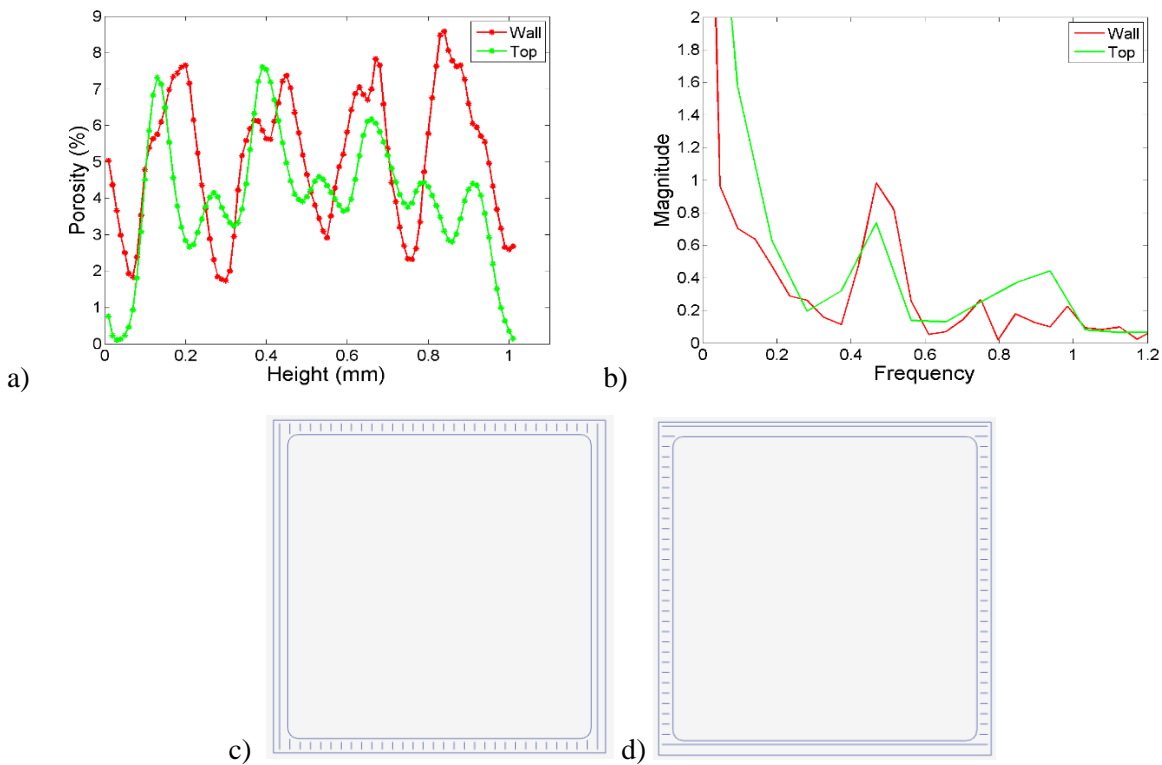
Figure 11 a) Porosity distribution along the printing direction for 2 different sintered regions indicated in Figure 8b (wall and top); b) Fourier transform of the porosity distribution shown in a; c) x and d) y cross scanning pattern used to produce the walls of the test object reported in Figure 2a.

3. Influence of the scanning pattern on the porosity characteristics

Among the different parameter sets used to produce the first test object, the four that warranty the best bonding between the layers, have been selected to be further assessed through the use of 4 different scanning pattern. According to Figure 9b, the four best parameter sets were: 1, 2, 4 and 5.

Figure 13a shows the array of scanning patterns which in combination with the parameter sets mentioned have been used to produce the cylinders of the second test object (see Figure 2b). The assessment of the different scanning strategies (parameters sets + scanning pattern) is performed through the measurement of the porosity content and the creation of a cumulative porosity map, which allow to spot the areas most affected by porosity. Figure 12 shows the workflow followed to obtain the porosity map shown in Figure 13b.
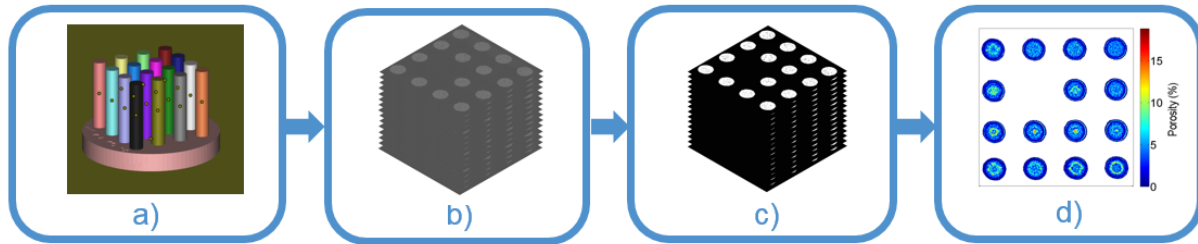
Figure 12 Workflow from the STL model of the second test object containing an array of cylinders (3mm diameter) used for the evaluation of influence of the scanning pattern on the porosity content and porosity distribution. a) STL model of the second test object; b) CT-slices exported along the printing direction; c) CT-slices binarized used to calculate the porosity content in each slice; d) Porosity map which resumes the porosity information of all the CT-slices along the printing direction.

Figure 13b shows how the influence of a certain scanning pattern leads to similar porosity map independently to the parameters set used. Scanning pattern A leads to the most uniform porosity distribution, without any particular area more affected by the porosity. Scanning pattern B leads to a higher concentration of porosity in the center of the cylinders compared to A, with more marked effect for higher power and scanning speed (the scanning B2 was set in a wrong way leading to an insufficient sintering of the powder). Scanning pattern C determines even a higher concentration of porosity in the center of the cylinders with an apparent formation of concentric rings of porosity. Scanning pattern D determines the formation of an internal ring of porosity probably due to the too high energy input in the area because of the overlap between the internal contour and the hatching vectors. Figure 14b shows the average radial porosity profiles of the cylinders manufactured using the parameter set 4. The peaks visible in the profiles refer to the ring of porosity described previously.
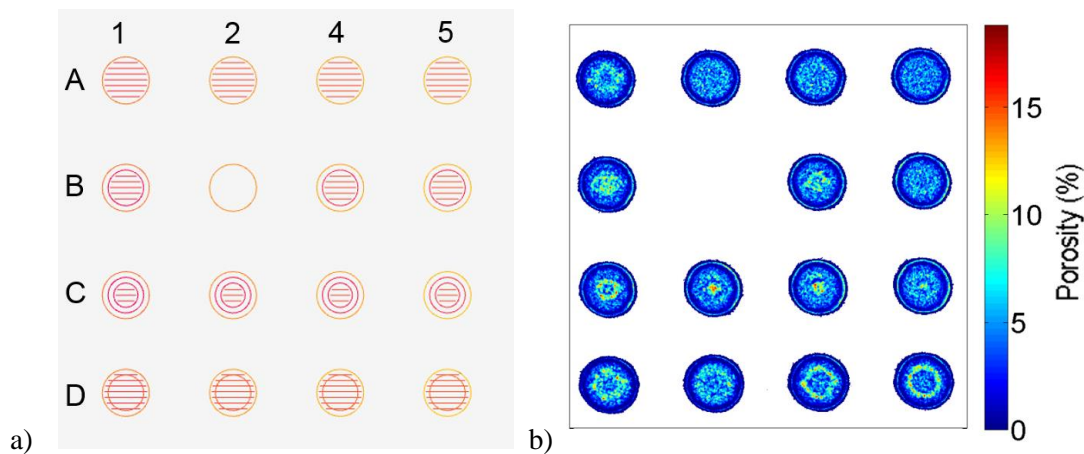
*Figure 13 a) Array of scanning patterns used to produce the second test object with references to the scanning order and the parameters sets used which are reported respectively in Table 2 and Table 3; b) Porosity map which shows the most affected area along the printing direction. *There was an error in the settings of the scanning pattern relative to the position B2.*

According to the porosity content of each cylinder shown in Figure 14a, the best scanning strategy is C2, with C being overall the best scanning pattern and 2 being the best parameter sets.
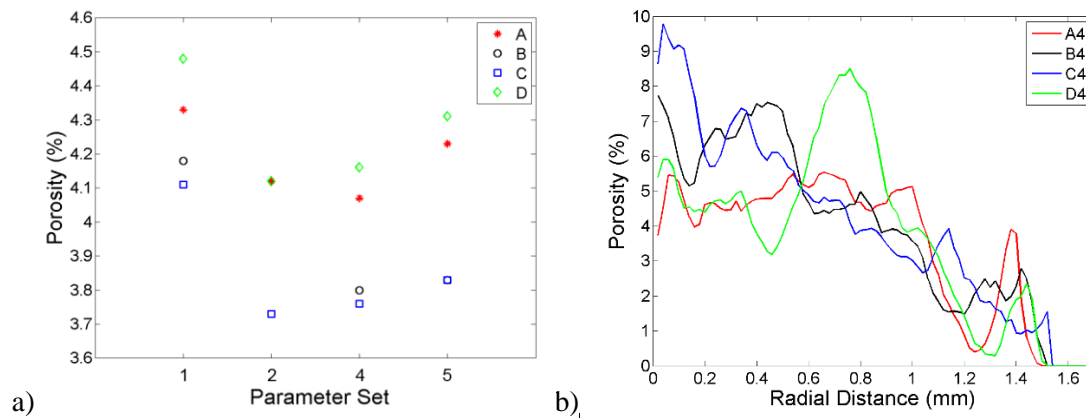
Figure 14 a) Porosity content of each cylinder of the second test object; b) Radial porosity profile for all the scanning pattern which use the parameter set 4 (see Table 3).

Conclusions

In this work a new approach for quality control of laser sintering of polymers at microscale level and scanning strategy (parameter sets + scanning pattern) assessment has been presented. The first part of the study shows how the use of the tools based on image processing allows to measure the porosity distribution within the part, estimate the sintered layer thickness and indirectly assess the stability of the sintering conditions at the layer thickness level. In the second part of the study was presented a first test object which allows to directly assess the bonding between the layers, the curling due to the crystallization of the polymer during solidification, the powder packing density and its local variation. The analysis proposed for this first test object allows to assess the process at microscale, giving important hints on the physics of the process. In the third part of the study a second test object is used to assess the influence of the scanning pattern for different parameters sets. This object constituted by an array of cylinders allow to assess up to 16 different scanning strategies by assigning each of them to a different cylinder. The creation of a porosity map together with the radial porosity profile allowed to point out the areas more affected by porosity and correlating them with the scanning pattern used. Besides pointing out some peculiar effect of the laser sintering process, the approach allowed to find an optimized scanning strategy which minimized the porosity content. Although the examples brought focused on PA12, the tools and the approach shown in the three parts of the study are general and can be applied to all polymeric powders available for laser sintering, allowing to make a direct link between process parameters, scanning pattern and defect's level in the microstructure. The approach presented could potentially be used to speed up the selection of the scanning strategy to apply while processing a new polymer, postponing the mechanical tests to the final iteration step. The small size of the sample reduces also the research effort related to the printing step (shorter build's height), reducing both machine and material's costs for the tests, allowing faster iterations in the parameter sets selection.

References

[1] Goodridge RD, Tuck CJ, Hague RJM, 2012, Laser sintering of polyamides and other polymers, Progress in Materials Science, 57/2:229-267.

[2] Vasquez GM, Majewski CE, Haworth B, Hopkinson N, 2014, A targeted material selection process for polymers in laser sintering, Additive Manufacturing, 127-138.

[3] Kruth JP, Levy G, Klocke F, Childs T, 2007, Consolidation phenomena in laser and powder-bed based layered manufacturing, CIRP Annals - Manufacturing Technology, Vol.56(2), 730-759.

[4] Usher JS, Gornet T J, Starr TL, 2013, Weibull growth modelling of laser sintered nylon 12. Rapid Prototyping Journal, 19/4:300-306.

[5] Beretta S, Evans KE, Ghita O, 2015, Processability of PEEK, a new polymer for High Temperature Laser Sintering (HT-LS), European Polymer Journal, Vol.68, 243-266.

[6] Wei Zhu et al., 2015, Investigation into mechanical and microstructural properties of polypropylene manufactured by selective laser sintering in comparison with injection molding counterparts, Materials and Design, 37-45.

[7] Bellehumeur CT et al.,1996 , An experimental study and model assessment of polymer sintering, Polymer Engineering and Science, 2198-2207.

[8] Haworth B, Hopkinson N, Hitt D, Zhong X, 2013, Shear viscosity measurements on PA-12 polymers for laser sintering. Rapid Prototyping Journal, Vol.19(1), 28-36.

[9] Faes M, Wang Y, Lava P, Moens D, 2015, Variability in the mechanical properties of laser sintered PA-12 components, Proc. Solid Free Form Symposium. Texas, August 10-12: 847-846.

[10] Kruth JP, Bartscher M, Carmignato S, Schmitt R, De Chiffre L, 2011, Computed tomography for dimensional metrology, CIRP Annals – Manufacturing Technology, 60/2: 821-842.

[11] Rouholamin D, Hopkinson N, 2015, An Investigation on the suitability of micro-computed tomography as a non-distructive technique to assess the morphology of laser sintered nylon parts. Journal of Engineering, 665

[12] Ghita O, James E, Trimble R, Evans KE, 2014, Physico-chemical behaviour of Poly (Ether Ketone) (PEK) in HighTemperature Laser Sintering (HT-LS), Journal of Materials Processing Tech., Vol.214(4), 969-978

[13] Ruesenberg S, Schmidt L, Schmid HJ, 2011, Mechanical and Physical properties - A way to asses quality of Laser Sintered Parts, SFF 2011:239-251.

[14] Dewulf W, Pavan M, Craeghs T and Kruth JP, 2016, Using X-ray Computed Tomography to improve the porosity level of polyamide-12 laser sintered parts, CIRP Annals - Manufacturing Technology

[15] Pavan M, Craeghs T, Kruth JP, Dewulf W, 2016, CT-based quality control of Laser Sintering of Polymers, iCT Conference, Wels, February 9-12.

[16] Pavan M, Craeghs T, Kruth JP, Dewulf W, 2016, CT-based quality control of Laser Sintering of Polymers, Case Studies in Nondestructive Testing and Evaluation, doi:10.1016/j.csndt.2016.04.004

[17] Pavan M, Craeghs T, Van Puyvelde P, Kruth JP, Dewulf W, 2016, Understanding the link between process parameters, microstructure and mechanical properties of laser sintered PA12 parts through X-ray computed tomography, Pro-AM conference, Singapore, May 16-19.

[18] http://software.materialise.com/control-platform

[19] Williams JD, Deckard CR, 1998, Advances in modeling the effects of selected parameters on the SLS process, Rapid Prototyping Journal, 4/90-100.

[20] Van Den Eynde M, Verbelen L, Van Puyvelde P, 2015, Assessing polymer powder flow for the application of laser sintering, Powder Technology, 286/151-155.